PLASMA MECHANISM OF RADIO EMISSION GENERATION ON A SHOCK WAVE IN THE VICINITY OF AN EXOPLANET

© 2025 A. A. Kuznetsov*, V. V. Zaitsev

Gaponov-Grekhov Institute of Applied Physics, Russian Academy of Sciences, Nizhny Novgorod, Russia.

**e-mail: kuznetsov.alexey@ipfran.ru*

Received February 23, 2025

Revised April 20, 2025

Accepted June 17, 2025

Abstract. The paper evaluates the possibility of efficient radio emission generation in the head shock region of "hot Jupiter" type exoplanets. A drift acceleration mechanism on the quasi-transverse shock wave is proposed as a source of energetic electrons. Electrons reflected from the shock wave and accelerated by it propagate in the relatively dense plasma of the stellar wind and generate plasma waves, so the plasma mechanism is considered as a source of radio waves. Using the example of the head shock of the hot Jupiter HD 189733b as an example, the parameters of the beam of energetic electrons, plasma waves, and the frequency of the generated radio emission are estimated. The energetic estimation of the region of stellar wind parameters, for which the registration of radio emission from the head shock wave of exoplanet HD 189733b by modern astronomical means is possible, is performed.

DOI: 10.31857/S00167940250714e1

1. INTRODUCTION

An important goal of modern radio astronomy research is to search for radio emission from exoplanets, the detection of which could provide numerous data on their plasma envelopes and shed light on the processes responsible for the formation of stellar systems. Exoplanet HD 189733b is a typical and one of the most studied representatives of "hot Jupiters", which have sizes comparable to Jupiterian and are located at a small distance (closer than 0.1 a.u.) from their parent stars. In this paper, using the example of exoplanet HD 189733b, we discuss the possibility of generating in the region of the head exoplanet shock wave a radio emission sufficient in intensity to be detected by modern radio astronomical means. For this purpose, the kinetic energy density W of the electron flux accelerated by a single reflection from the exoplanet shock wave via the drift mechanism is estimated on the one hand (Wu, 1984; Mann and Klassen, 2005). The considered parameters of the

stellar wind are such that the propagation of high-energy electrons in it leads to the development of Langmuir instability, i.e., the excitation of plasma waves (Mikhailovsky, 1971; Treumann, 1997). Therefore, on the other hand, the energy density of these waves W , necessary for generation by means of the plasma mechanism (Zaitsev and Stepanov, 1983), sufficiently intense to register radio emission, is estimated. From the condition $W \gg W$, the paper estimates the region of stellar wind parameters at which the detection of radio emission from the exoplanet shock region is energetically feasible. The frequency range in which the radio emission is generated will also be estimated.

According to the available work on numerical gas dynamic and MHD modeling of the HD 189733 system, the stellar wind velocity v_s relative to the exoplanet can both exceed the magnetosonic velocity v_{ms} and yield to it during the orbit of HD 189733 b (Fares et al. 2017, Strugarek et al. 2022, Kavanagh et al. 2019, Odert et al. 2020, Rumenskikh et al. 2022). At $v_{ms} > v_s$ the head shock may be absent (Zhilkin and Bisikalo, 2019). Then, at a weak exoplanet magnetic field, the colliding stellar wind penetrates the plasmasphere, in which there is a sufficient number of neutral particles, the different frequency of collisions of electrons and ions with which provides charge separation and, consequently, the emergence of the electron-accelerating component of the electric field (Zaitsev et al., 2024). In the present work, we consider the case $v_s > v_{ms}$, in which an exoplanet head shock wave is formed and the mechanism of drift acceleration of electrons is realized in its region where it is quasi-transverse, i.e., the angle θ between the normal to the shock wave and the magnetic field of the stellar wind is close to 90° . The fast magnetosonic shock wave is accompanied by a compression of the magnetic field, so it acts as a moving magnetic mirror from which electrons are uniquely reflected and accelerated. This mechanism has been widely discussed in studies of electron acceleration in Earth's head shock (Wu, 1984; Holman and Pesses, 1983; Liu et al. 2022), interplanetary shock waves (Yang et al., 2024), and coronal shock waves generating type II radio bursts (Mann and Klassen, 2005; Ball and Melrose, 2001; Mann et al., 2018).

By analogy with solar system planets, an electron cyclotron maser is often proposed as a mechanism for radio emission generation by accelerated electrons, which, however, is effective when the electron gyro frequency significantly exceeds the plasma frequency $\Omega_c \gg \omega_p$ (Wu and Lee, 1979; Melrose et al., 1984, Louis et al., 2019). For the stellar wind in the orbit of exoplanet HD 189733b, the inverse relationship $\Omega_c \ll \omega_p$ is true, so a plasma mechanism for radio emission generation may be effective (Zaitsev and Stepanov, 1983; Zaitsev and Shaposhnikov, 2022). This mechanism involves the generation of plasma waves by energetic electrons and their subsequent conversion into electromagnetic radiation at the plasma frequency by scattering on plasma particles (Rayleigh scattering) or at twice the plasma frequency as a result of the merging of plasma waves (Raman scattering). The possible frequency range of radio emission in this model is determined not by the magnitude of the magnetic field in the source, but by the concentration of stellar wind

plasma n on the exoplanet shock wave.

In the case of Rayleigh scattering, which occurs most efficiently on background plasma ions, under certain conditions there is a maser effect, manifesting itself in an exponential growth of the electromagnetic radiation intensity with increasing plasma wave energy. In Raman scattering, the maser effect is absent due to the decay of the electromagnetic wave into two plasma waves at high radio emission intensities. Nevertheless, the values of the brightness temperature in the source required to provide the observed radio emission flux can be comparable in the cases of Rayleigh and Raman scattering (Zaitsev and Stepanov, 1983; Zheleznyakov, 1996; Zaitsev et al., 2023).

Section 2 is devoted to a brief description of the mechanism of electron drift acceleration on a quasi-transverse shock wave. In Section 3, the kinetic energy density of fast electrons accelerated on the shock wave of exoplanet HD 189733b is estimated for different stellar wind parameters. In Section 4, we present estimates of the spectrum of plasma waves generated by energetic particles. Section 5 briefly discusses the Rayleigh and Raman mechanisms for the conversion of plasma waves to electromagnetic waves, and provides estimates for the plasma wave energy density required to produce the radio emission flux detected on Earth. A comparison of the estimates of the plasma wave energy density and the kinetic energy of accelerated electrons allows us to determine the region of stellar wind parameters in which the observation of radio emission due to electron acceleration in the head shock wave of exoplanet HD 189733b is energetically feasible.

2. DRIFT MECHANISM OF ELECTRON ACCELERATION ON THE SHOCK WAVE

Consideration of the acceleration mechanism is possible in the nonrelativistic approximation, since the velocity of the reflected electron beam subsequently appears to be. It is convenient to describe the drift mechanism of electron acceleration in the reference frame introduced by De Hoffmann-Teller (Fig. 1), in which there is no induced electric field, since the stellar wind velocity in this system is co-directed with the magnetic field (Ball and Melrose, 2001; De Hoffmann and Teller, 1950). Since the fast magnetosonic shock wave is accompanied by compression of the magnetic field, the scale of inhomogeneity of which is much larger than the electron gyroradius, the shock wave plays the role of a magnetic mirror moving along the lines of force with the velocity $v_s \sec\theta$. Then the electrons not caught in the loss cone can be reflected and accelerated by it once. The electron velocity components along the magnetic field before and after reflection, $v_{i,\parallel}$ and $v_{r,\parallel}$ respectively, are related by the relation (1).

$$v_{r,\parallel} = 2v_s \sec\theta - v_{i,\parallel}. \quad (1)$$

where $v_s = \sqrt{v_{sw}^2 + v_{orb}^2}$ is the stellar wind velocity with respect to the shock wave, equal to the rms of the stellar wind velocity at the exoplanet orbit v_{sw} and the intrinsic velocity of the orbital motion

of HD 189733b v_{orb} , which is no longer negligibly small as for the planets of the Solar System (Vidotto et al., 2010). From (1) we see that the velocity increment in the reflection of an individual electron is proportional to the stellar wind velocity and increases as the angle approaches 90° . Transverse to the magnetic field, the velocity $v_{\perp}$ at reflection remains unchanged.

For solar wind electrons, it is known that their velocity distribution in the high velocity region declines in a stepwise fashion (Echim et al., 2010; Dudik et al., 2017; Kuznetsov et al., 2018), and their temperature can differ from the ionic temperature both upward and downward (Shi et al., 2023). However, due to the lack of detailed data and for simplicity, electrons in the source plasma of the stellar wind HD 189733 in an exoplanet orbit are assumed to have a Maxwellian isotropic velocity distribution (2) and the same temperature as ions T :

$$f_{bkg}(v_{\perp}, v_{\parallel}) = \frac{1}{(2\pi v_{th})^{\frac{3}{2}}} \exp\left(-\frac{v_{\perp}^2 + v_{\parallel}^2}{2v_{th}^2}\right), \tag{2}$$

where $v_{th} = \sqrt{\frac{k_b T}{m_e}}$ is the thermal velocity of stellar wind electrons. In such a case, the distribution of reflected electrons takes the form:

$$f_{acc}(v_{\perp}, v_{\parallel}) = \frac{\Theta(v_{\parallel} - v_s \sec\theta)\Theta(v_{\perp} - v_{\perp,lc})}{(2\pi v_{th})^{\frac{3}{2}}} \exp\left(-\frac{v_{\perp}^2 + (v_{\parallel} - 2v_s \sec\theta)^2}{2v_{th}^2}\right), \tag{3}$$

Where $\Theta(x)$ is the Heaviside function, so that $\Theta(x) = 1$ at $x > 0$ and $\Theta(x) = 0$ at $x < 0$, and $v_{\perp,lc} = \tan\alpha_{lc}\sqrt{(v_{\parallel} - v_s \sec\theta)^2 + V_e^2}$, where the effective velocity $V_e = \sqrt{\frac{2e\phi_{HT}}{m_e}}$, related to the electrostatic potential ϕ_{HT} **(7),** is introduced**.** The pitch angle α_{lc} is defined by the expression $\alpha_{lc} = \arcsin\left[\left(\frac{B_1}{B_2}\right)^{\frac{1}{2}}\right]$, where B_1 and B_2 are the magnetic field strengths before and after the shock. In the MHD approximation based on the Rankine-Hugoniot relations (Priest, 1982), the slug ratio $X = \frac{B_1}{B_2}$ for the transverse shock wave obeys the equality (4):

$$aX^{-2} + bX^{-1} + c = 0, \tag{4}$$

in which

$$a = 2 - \gamma,\ b = \left(\frac{2c_s^2}{\gamma v_a^2} + (\gamma - 1)\frac{v_s^2}{\gamma v_a^2} + 1\right)\gamma,\ c = -(\gamma + 1)\frac{v_s^2}{v_a^2}, \tag{5}$$

where the Alfvenov velocity $v_a^2 = \frac{B^2}{4\pi n m_i}$ and the speed of sound $c_s^2 = \frac{\gamma k_b T}{m_i}$, with the adiabatic exponen t $\gamma = \frac{5}{3}$, are introduced. In the dense stellar wind providing $b^2 \gg 4ac$ and $v_a^2 \ll v_s^2$, the magnitude of the slug ratio is independent of the **plasma** concentration and the magnetic field **there**

in (6):

$$X \approx -\frac{b}{c} \approx \frac{2c_s^2 + (\gamma - 1)v_s^2}{(\gamma + 1)v_s^2}. \quad (6)$$

Due to the different inertia of protons and electrons across the shock, an electrostatic potential ϕ_{HT} (Goodrich and Scudder, 1984) is established across the shock, equal to:

$$e\phi_{HT} = \frac{\gamma}{\gamma - 1} k_b T. \quad (7)$$

The velocity distribution of accelerated particles (3) belongs to the family of cone distributions with a shift (Wu, 1984). Its value is different from zero if two conditions are fulfilled: the particle velocity does not exceed the shock wave velocity along the force line $v_{\parallel} > v_s \sec\theta$ and the particle does not fall into the loss cone $v_{\parallel} > v_{\parallel,lc}$.

3. ELECTRON ACCELERATION ON THE SHOCK WAVE OF THE EXOPLANET HD 189733B

The star HD 189733 belongs to the orange dwarf class with radius $R_{star} \approx 0.76 R_{\odot}$ and possesses a hot Jupiter-type exoplanet orbiting $\approx 9 R_s$. At such distances, the stellar wind turns out to be significantly inhomogeneous in azimuth in the plane of the planet's orbit due to the inhomogeneous outflow of matter from the star's surface. Then, as follows from MHD modeling (Fares et al., 2017, Strugarek et al., 2022, Odert et al., 2020), at least part of the planet's orbit lies in a region where the relative velocity of the stellar wind and exoplanet v_s exceeds the fast magnetosonic velocity v_{ms}:

$$v_s = \sqrt{v_{sw}^2 + v_{orb}^2} > v_{ms} = \sqrt{v_a^2 + c_s^2}. \quad (8)$$

Inequality (8) is a condition for the generation of the fast magnetosonic shock wave (Priest, 1982) required for the drift acceleration of electrons (Section 2).

The shape, position, and type of the exoplanet head shock wave are the subject of active research and depend significantly on the stellar wind parameters (Rumenskikh et al., 2022; Zhilkin and Bisikalo, 2019; Vidotto et al., 2010; Llama et al., 2013; Bourrier et al., 2013). Thus, depending on its intensity, the shock can be located between 3 and 20 exoplanet radii away from the center of HD 189733b. The smallest distance is reached at a coronal mass ejection on the parent star, which corresponds to the values of stellar wind parameters from the N4 set (Odert et al., 2020). Set N3 consisted of the values of stellar wind parameters that are the most optimal for drift acceleration among those observed in the exoplanet orbit in MHD modeling (Odert et al., 2020). The N2 set consists of average values of the stellar wind parameters from the data (Kavanagh et al., 2019). Finally, set N1 uses the stellar wind parameters in one of the gasdynamical calculations (Rumenskikh et al., 2022) with the addition of a relatively weak magnetic field $B = 0.01$ Gs, at which the magnetosonic shock wave is formed and the loss cone is not too large, so that the

acceleration mechanism is quite efficient. In this section of the paper, we first estimate the value of the kinetic energy density of accelerated electrons normalized by their thermal energy (12) for selected sets of parameters, and then study the dependence of this value on the concentration n , velocity v_{sw} , and magnetic field B of the stellar wind at the characteristic temperature $T = 1.5 \cdot 10^6$ K.

By integrating the distribution (3) of accelerated particles in velocity space, expressions can be found for their concentration n_{acc} and the characteristic longitudinal $v_{b,\parallel}$ and transverse $v_{b,\boxplus}$ velocities of the reflected particle beam as a function of the angle between the magnetic field and the normal to the shock θ (Mann and Klassen, 2005).

$$\frac{n_{acc}(\theta)}{n} = \exp\left(-\frac{v_s^2 \sec^2\theta \sin^2\alpha_{lc} + V_s^2 \tan^2\alpha_{lc}}{2v_{th}^2}\right) \cdot \frac{\cos\alpha_{lc}}{2}\left(1 + \operatorname{erf}\left(\frac{\sqrt{2}v_s \sec\theta \cos\alpha_{lc}}{v_{th}}\right)\right), \tag{9}$$

$$v_{b,\parallel}(\theta) = v_s \sec\theta\left(1 + \cos^2\alpha_{lc}\right), \tag{10}$$

$$v_{b,\boxplus}(\theta) = \tan\alpha_{lc}\sqrt{\left(v_{b,\parallel} - v_s \sec\theta\right)^2 + V_s^2}. \tag{11}$$

Dimensionless energy density of accelerated electrons, defined as

$$W(\theta) \approx \frac{m_e n_{acc}\left(v_{b,\parallel}^2 + v_{b,\boxplus}^2\right)}{2nk_bT} \tag{12}$$

at $v_s \sin\alpha_{lc} \ll \sqrt{2}v_{th}$ is maximal for the value of the angle $\theta_{max\square}$, close to 90° (14). Therefore, the range of angles at which the energy density is comparable to the maximum is estimated as $\Delta\theta \approx 90^\circ - \theta_{max\square}$ and is approximately equal to $\approx 5^\circ \div 15^\circ$ for the parameters used (Fig. 2). The maximum energy density $W(\theta_{max\square})$ and the corresponding angle $\theta_{max\square}$ are under the assumption $\frac{\sqrt{2}v_s \sec\theta \cos\alpha_{lc}}{v_{th}} \gg 1$ (13-14). The value of the maximum energy density $W(\theta_{max\square})$ depends solely on the pitch angle α_{lc} (13), through the determination of which the energy value $W(\theta_{max\square})$ is affected by the stellar wind parameters, and decreases monotonically as it increases (Fig. 3). For the selected parameter sets, the pitch angle value increases from 32° to 43° , which leads to an order of magnitude decrease in the maximum energy density $W(\theta_{max\square})$ (Table 2).

$$W(\theta_{max\square}) \approx \cos(\alpha_{lc})\left(\left(\frac{1+\cos^2\alpha_{lc}}{\sin\alpha_{lc}}\right)^2 + \tan^2\alpha_{lc}\left(\frac{\cos^2\alpha_{lc}}{\tan^2\alpha_{lc}} + \frac{\gamma}{\gamma-1}\right)\right)\exp\left(-1 - \frac{\gamma\tan^2\alpha_{lc}}{2\gamma-2}\right) \tag{13}$$

$$\theta_{max} = \arccos\sqrt{\frac{v_s^2\sin^2\alpha_{lc}}{2v_{th}^2}}. \tag{14}$$

The magnitude of the pitch angle α_{lc} at low Alfvénova velocity of the stellar wind $v_a \ll v_s$ depends only on its temperature and flux rate (6). Therefore, the dimensionless energy density of accelerated electrons $W(\theta_{max\square})$ tends to an asymptote as the concentration n increases (Fig. 4). As

the magnetic field of the stellar wind B increases and its velocity v_s decreases, the energy density $W(\theta_{max})$ decreases.

4. PLASMA WAVE GENERATION

The electrons reflected from the shock wave return to the unmagnetized $(\omega_p \gg \omega_c)$ stellar wind plasma, so the full distribution function when the angle between the normal to the shock wave and the magnetic field $\theta = \theta_{max}$, close to the optimum, is realized, takes the form:

$$f(v_\parallel, v_\perp, \theta_{max}) = f_m(v_\parallel, v_\perp) + f_{acc}(v_\parallel, v_\perp, \theta_{max}). \quad (15)$$

Although the full distribution function is axially symmetric, its two-dimensional slice in $(v_\parallel, v_\perp)$ coordinates can be interpreted as an energetic beam of accelerated electrons propagating in the warm and dense stellar wind plasma. Expressions for both components of the beam flux velocity v_b are given in Section 3. The thermal spread of particles in the beam is, strictly speaking, not isotropic, but since their source is the same stellar wind, it will be assumed to be equal to the background thermal velocity in the estimates below v_{th}. Since $v_b \geq \sqrt{3} v_{th}$, for all values of the parameters used, there exists a range of particle velocities in which the inequality $\frac{\partial f}{\partial |v|} > 0$ is valid, so that due to beam instability (Mikhailovsky, 1971; Treumann, 1997), Langmuir (plasma) waves with a frequency ω_p equal to:

$$\omega_p^2 \approx \omega_L^2 + 3k^2 v_{th}^2, \quad (16)$$

where $\omega_L^2 = \frac{4\pi n e^2}{m_e}$. The range of velocities in which the inequality $\frac{\partial F}{\partial |v|} > 0,$ is satisfied for the electron distribution function can be roughly estimated as $v \in (v_b - v_{th}; v_b)$. Then, using the resonance condition $\omega_p \approx kv$, an estimate (17) is obtained for the range of unstable wave numbers k (and consequently, frequencies f_p) of evolving plasma waves:

$$k_p \in (k_{p,min}; k_{p,max}) = \left(\frac{\omega_L^2}{(v_b - v_{th})^2 - 3v_{th}^2}; \frac{\omega_L^2}{v_b^2 - 3v_{th}^2} \right). \quad (17)$$

From here, the characteristic wave number of the spectrum $\langle k_p \rangle$ and the width of the range of unstable wave numbers Δk_p can be estimated:

$$\langle k_p \rangle \approx \frac{k_{p,min} + k_{p,max}}{2}, \quad \Delta k_p \approx k_{p,max} - k_{p,min} \quad (18)$$

For the development of Langmuir instability it is necessary that its increment exceeds the effective frequency of electron-ion collisions ν_{ei}, determined by the formula (Zheleznyakov, 1996):

$$\nu_{ei} = \sqrt{\frac{8\pi}{m_e}} \frac{e^4 n}{(k_b T)^{\frac{3}{2}}} \ln\left(0.37 \frac{k_b T}{e^2 n^{\frac{1}{3}}}\right) \approx 50 \frac{n[\text{см}]}{T[\text{эВ}]^{\frac{3}{2}}} \quad (19)$$

With the stellar wind parameters used in this work, the condition $\gamma_{max} \gg \nu_{ei}$ is fulfilled. We also note that as a result of scattering of plasma waves by stellar wind particles, their spectrum is

isotropic. Therefore, without loss of generality, we can for simplicity assume that the spectrum of plasma waves is isotropic with spectral density W_k . In this case, the total energy density of plasma waves is determined by the formula $W_p = \int W_k dk$.

5. TRANSFORMATION OF PLASMA WAVES INTO RADIO EMISSION

Excited plasma waves with frequency ω_p are transformed into radiation by scattering on stellar wind particles (Rayleigh scattering). The conservation law is of the form:

$$\omega_t - \omega_p = (\mathbf{k}_t - \mathbf{k}_p)\mathbf{v}, \tag{20}$$

where w_t and $\mathbf{k}_t$ are the frequency and wave vector of the electromagnetic wave, $\mathbf{v}$ is the velocity of the scattering particle. Rayleigh scattering leads to radio emission with frequency $\omega_t \approx \omega_p$. Nonlinear interaction of two plasma waves (Raman scattering)

$$\omega_p + \omega_p' = \omega_t, \ \mathbf{k}_p + \mathbf{k}_p' = \mathbf{k}_t \tag{21}$$

generates radio emission at the second harmonic of the plasma frequency .

To characterize the intensity of radiation from space objects, radio astronomy uses the brightness temperature T_b . This value is related to the radio wave flux F , measured at a distance R_{se} from the source, by the following relation (Zheleznyakov, 1996):

$$F = \frac{2\omega_t^2 k_b T_b}{(2\pi c)^2} \frac{R_s^2}{R_{se}^2}, \tag{22}$$

where R_s is the characteristic size of the source within line of sight. Since the primary cause of radio waves are electrons accelerated on the quasi-transverse exoplanet shock wave, the value of R_s is equal to the characteristic linear size of the shock wave. As is clear from estimates and numerical simulations, the location, shape, and type of the exoplanet shock wave depend significantly on the stellar wind parameters (Zhilkin and Bisikalo, 2019), so a rather cautious estimate is used for its linear size $R_s \approx LR_p \sin(\Delta\theta)$ where R_p is the radius of exoplanet HD 189733b, $\Delta\theta$ is the spread of values of the angle between the normal to the shock wave and the magnetic field, where the acceleration mechanism is effectively realized and roughly estimated as $\Delta\theta \approx 90^\circ - \theta_{max}$ (Fig. 2).

The variation of the brightness temperature T_b along the propagation beam is described by the transport equation:

$$\frac{dT_b}{dl} = a_i - (\mu_{Ni} + \mu_C)T_b. \tag{23}$$

Let for Rayleigh scattering $i = 1$, and for Raman scattering $i = 2$. In equation (23), the coefficient a_i represents spontaneous scattering, and μ_{N1} represents induced scattering of plasma waves on electromagnetic waves, μ_{N2} is the nonlinear absorption coefficient of the electromagnetic wave, and μ_C is the absorption coefficient due to Coulomb collisions. In subsections 5.1 and 5.2, the

relationship between the dimensionless plasma wave energy density $W_i = \frac{W_p}{nk_bT}$ and the radio wave flux F , measured on Earth, will be derived using equations (22) and (23). Further, in subsection 5.3, the minimum flux value detected by modern radio telescopes will be substituted into the derived relations and an estimate of the plasma wave energy density W_i necessary for radio wave registration on Earth will be obtained both in the case of Rayleigh and Raman scattering. In the following, from the condition $W \gg W_i$ the stellar wind parameters at which the detection of radio emission from the exoplanet shock region is energetically possible will be estimated.

5.1 Rayleigh scattering.

If the induced scattering coefficient μ_{N1} is negative and sufficiently large in absolute value $(|\mu_{N1}| > \mu_C)$, then the total coefficient in the right-hand side of equation (23) becomes negative. In this case, the induced effect for Rayleigh scattering becomes dominant, and an exponential increase in the brightness temperature T_b is observed as the plasma wave energy density increases. This phenomenon is known as plasma maser. The efficiency of maser amplification of electromagnetic waves is determined by the optical depth of the source τ :

$$\tau = \int_0^{R_s} |\mu_{N1} + \mu_C| dl \tag{24}$$

In the case of Rayleigh scattering at appropriate plasma wave energy densities, the optical depth τ can reach high values, providing significant radio emission fluxes from the source (Zaitsev and Shaposhnikov, 2022).

As mentioned above, the conversion process (20) is most efficient when the plasma waves are scattered by the main plasma ions. At such scattering, the frequency change in each act is insignificant. In this case, the scattering has a differential character: the width of the plasma wave spectrum is larger than the width of the kernel of the integral equation describing induced scattering (Zheleznyakov, 1996). The coefficients of spontaneous (a_1) and induced (μ_{N1}) scattering, used in equation (23), in the case of an isotropic plasma wave spectrum have the following form (Tsytovich, 1977):

$$a_1 = \frac{\pi}{36} \frac{\omega_L^3 W_k}{v_g n v_{th}^2 k_p} \tag{25}$$

$$\mu_{N1} = -\frac{\pi}{108} \frac{m_e \omega_L^3}{m_i v_g n k_b T v_{th}^2 k_p} \frac{\partial}{\partial k_p} (k_p W_k) \tag{26}$$

The collisional absorption coefficient (μ_{C1}) is determined by the formula (Ginzburg, 1970):

$$\mu_C = \frac{\omega_L^2 \nu_{ei}}{\omega_t^2 v_g} \tag{27}$$

$$v_g = c\sqrt{1-\frac{\omega_L^2}{\omega_t^2}} = \sqrt{3}ck_p v_{th}$$

In equations (25)-(27) ω_p is the group velocity of electromagnetic waves with frequency $\omega_t^2 \approx \omega_p^2 = \omega_L^2 + 3k_p^2 v_{th}^2$ in the region of plasma wave generation, $\omega_t = 2\pi f_t$ is the frequency of electromagnetic wave, ν_{ei} is the frequency of electron-ion collisions (19).

When solving equation (23), it is convenient to switch from integration over the spatial coordinate l along the radiation propagation to integration over the plasma wave vector from $k_{p,min}$ to $k_{p,max}$. Given that $\omega_p = const$, we obtain the following relation between dl and dk_p:

$$dl = 6L_n \frac{v_{th}^2}{\omega_p^2} k_p dk_p, \tag{28}$$

where $L_n = \left| n\left(\frac{dn}{dl}\right)^{-1} \right|$ is the characteristic scale of the plasma inhomogeneity, which is estimated as $L_n \approx R_s \approx LR_p \sin(\Delta\theta)$. Then from (26) for the optical thickness of the induced scattering of plasma waves into electromagnetic τ_{N1}, an expression is obtained for the optical thickness of the induced scattering of plasma waves into electromagnetic:

$$\tau_{N1} = \int_0^{R_s} \mu_{N1}\, dl \approx -\frac{\pi}{18\sqrt{3}} \frac{m_e \omega_L \langle v_{ph} \rangle}{m_i c v_{th}} R_s W_1, \tag{29}$$

where $W = \frac{W_p}{nk_b T}$ is the ratio of the plasma wave energy density to the plasma thermal energy density, $\langle v_{ph} \rangle = \frac{\omega_p}{\langle k_p \rangle}$. A negative value of the optical thickness τ_{N1} indicates the possibility of an exponential dependence of the brightness temperature T_b of electromagnetic radiation on the plasma wave energy density.

The optical thickness of electromagnetic wave absorption due to Coulomb collisions in the plasma wave generation region is equal to:

$$\tau_{C1} = \int_0^{R_s} \mu_C\, dl \approx \frac{6}{\sqrt{3}} \frac{v_{th} \nu_{ei}}{c\langle v_{ph} \rangle} R_s \tag{30}$$

As mentioned above, maser amplification of electromagnetic radiation occurs when the induced conversion of plasma waves into electromagnetic waves exceeds the collisional absorption of electromagnetic waves, that is, for maser amplification to occur, the energy density of plasma waves must exceed a certain threshold, which is found from the condition $|\tau_{N1}| \gg \tau_{C1}$ (Zaitsev and Shaposhnikov, 2022):

$$W_1 \gg \frac{108}{\pi} \frac{m_i v_T^2 \nu_{ei}}{m_e \langle v_{ph}^2 \rangle \omega_L} \tag{31}$$

The solution of the transport equation (23) is:

$$T_b = \frac{a_i}{\mu_{Ni} + \mu_C}\left(1 - \exp(-\tau_C - \tau_{Ni})\right). \quad (32)$$

Therefore, if the condition (31) is satisfied, the expression for the observed radio flux F , arising from Rayleigh scattering of plasma waves generated by electrons accelerated during reflection from the exoplanet shock wave, takes the form:

$$F = 3\frac{k_b T m_i}{c^2 m_e} f_t^2 \frac{R_s^2}{R_{SE}^2} \cdot \left(\exp\left(\frac{\pi}{18\sqrt{3}} \frac{m_e \omega_p \langle v_{ph}\rangle}{m_i c v_{th}} R_s W_1\right) - 1\right) \exp(-\tau_{ext}), \quad (33)$$

where it is taken into account that on the path from the source to the observer **the radio emission** is subject to collisional absorption with optical thickness τ_{ext} . The estimates below are made assuming $\tau_{ext} \ll 1$.

5.2 Raman scattering

In Raman scattering of light, electromagnetic waves are generated with twice the plasma frequency $\omega_t = \omega_p^{(1)} + \omega_p^{(2)} \approx 2\omega_p$ and a wave vector of $\mathbf{k}_t \approx \mathbf{k}_p^{(1)} + \mathbf{k}_p^{(2)}$. The frequency$\omega_t$ and wave number$\mathbf{k}_t$ of an electromagnetic wave are related by the relationship $\omega_t^2 = \omega_L^2 + k_t^2 c^2$.

In the case of Raman scattering, the exponential dependence of the electromagnetic radiation intensity on the plasma wave energy density is not realized, because as the electromagnetic radiation density increases, the reverse process - attenuation of the electromagnetic wave at twice the plasma frequency with the formation of two plasma waves with frequency ω_p - begins to play an essential role. This process is equivalent to the appearance of effective scattering of electromagnetic waves (Zaitsev and Stepanov, 1983) and is characterized in the transport equation (23) by the nonlinear absorption coefficient μ_{N2} . The collisional absorption coefficient μ_C is determined by the same expression (27) as for Rayleigh scattering. In the case of an isotropic plasma wave spectrum, the coefficients of spontaneous emission and nonlinear absorption in the transport equation are of the form (Zaitsev et al., 2023):

$$a_2 = \frac{(2\pi)^5}{15\sqrt{3}} \frac{c^3}{\omega_L^2 \langle v_{ph}\rangle} \frac{W_2^2}{\xi^2} nT, \quad \mu_{N2} = \frac{(2\pi)^2}{5\sqrt{3}} \frac{\omega_L}{\langle v_{ph}\rangle} \frac{W_2}{\xi}, \quad (34)$$

where the parameter $\xi = \frac{c^3 (\Delta k)^3}{\omega_L^3}$ characterizes the spectral volume of plasma waves. Under the assumption of an isotropic spectrum of plasma waves for the parameter ξ , the following estimate is valid

$$\xi \approx \frac{4\pi c^3}{\omega_L^3 \langle k_p\rangle^2 \Delta k_p}, \quad (35)$$

in which the multipliers $\langle k_p\rangle$ and Δk_p are estimated earlier (18). Restricting ourselves to the case of greatest interest, in which the density of plasma waves is high enough so that $\mu_{N2} \gg \mu_C$ in the approximation of an optically thick source (Zaitsev et al., 2023), we obtain an estimate (36) of the

observed radio flux on Earth, generated due to Raman scattering:

$$F = \frac{2k_t^2 k_b}{(2\pi)^2}\frac{R_s^2}{R_{se}^2}\frac{a_2}{\mu_{N2}}\exp(-\tau_{ext}) = \frac{k_t^2 n k_b T}{3}\frac{R_s^2}{R_{se}^2}\frac{W_2}{(k_p^2)(k_{max}-k_{min})}\exp(-\tau_{ext}). \quad (36)$$

5.3 Transformation into radio emission of plasma waves generated by the accelerated head shock of exoplanet HD 189733b

The frequency of radio emission generated due to Rayleigh and Raman scattering is determined by the frequency of plasma waves ω_p , which slightly exceeds the Langmuir frequency ω_L , and varies from 3 to 40 MHz (see Table 3 and Fig. 8). The most effective radio astronomical instruments in this frequency range are UTR-2 (Ukrainian T-shaped Radio Telescope-2)[1] , LOFAR (LOw Frequency ARray) and NDA (Nançay Decameter Array). The sensitivity (minimum radiation flux that can be recorded with a 1 hour exposure time and a bandwidth of 4 MHz) of the UTR-2 radio telescope is 0.01 Jan in the range from 10 to 40 MHz, of the NDA radio telescope is 1 Jan in the range from 10 to 120 MHz (Fig. 5). The LOFAR sensitivity improves from 0.1 Yan to 0.005 Yan with increasing frequency from 15 MHz to 40 MHz (Grießmeier et al., 2011). Therefore, for further evaluations over the entire frequency range, the magnitude of the detected radio flux F in expressions (33) and (36) is taken to be 0.01 Yang.

The minimum plasma wave energy estimated from formula (33), which provides on Earth the radio flux $F = 0.01$ Yang due to Rayleigh scattering, W_1 turns out to be significantly lower than the energy of the accelerated electron beam for all four sets of parameters (see Sect. 3), characteristic according to various works for the stellar wind near the exoplanet shock (cf. Table 2 and Table 3). For the N1 set, the ratio $\frac{W_1}{W}$ turned out to be the smallest and approximately equal to 0.6. In other cases, the required plasma wave energy W_1 turned out to be 1-2 orders of magnitude lower than the estimated energy of accelerated electrons. For sets N1 and N3, the radio emission frequencies were 3.2 MHz and 6.9 MHz, which is below the ionospheric cutoff frequency of about 10 MHz (Grießmeier et al., 2011). In contrast, for the other two sets, the radio emission frequency was found to be approximately equal to 20 MHz. So, for the stellar wind parameter sets N2 and N4, characterized by the highest stellar wind densities, the observation of radio emission from Rayleigh scattering of plasma waves in the exoplanet shock region is energetically and frequency feasible.

The ratio of the minimum energy of plasma waves, providing on the Earth the radio emission flux $F = 0.01$ Yang due to Raman scattering, to the energy of accelerated electrons $\frac{W_2}{W}$ (the

[1] Probably damaged as a result of military actions on the territory of Ukraine. The authors of the paper have no reliable information about the current state of the radio telescope

value W_2 is estimated from (36)) only for the set N4 was significantly lower than 1, which indicates that it is impossible to observe on the Earth radio emission of this nature at other considered sets of stellar wind parameters.

As discussed earlier, the stellar wind in the orbit of HD 189733b is significantly inhomogeneous, so it is important to indicate the dependence of the possibility of effective radio emission generation at the main and doubled plasma frequencies depending on its parameters. At stellar wind concentration in the interval from $10^5 см^{-3}$ to and characteristic temperature $T = 1.5 \cdot 10^6$ K, the plasma wave energy W_1 , necessary for effective radio wave generation by Rayleigh scattering, decreases with increasing magnetic field and stellar wind velocity. Moreover, as its concentration increases, the dependence of the plasma wave energy on the magnetic field disappears, and the value under discussion turns out to be inversely proportional to approximately $\sqrt{n}$ (Fig. 6). Thus, at extremely high stellar wind velocity $v_{sw} = 1000$ km/s, the condition of effective radio wave generation $W \gg W_1$ is fulfilled already at a concentration of $n \geq 2 \cdot 10^5 см^{-3}$ and magnetic field up to 0.1 Gs. At stellar wind speed $v_{sw} = 500$ km/s the same is true for magnetic fields up to 0.04 Gs, and at $v_{sw} = 250$ km/s the condition of effective generation for the same magnetic fields is fulfilled only at $n \geq 3 \cdot 10^6 см^{-3}$ (cf. Fig. 4 and Fig. 6). It is important to note that in the case of Rayleigh scattering due to the maser effect, the energy density of plasma waves $W \gg W_1$ depends logarithmically on the minimum radio flux detected by the receiver, F (33), so that a degradation of the sensitivity to 1 Yang (which, for example, is possessed by the NDA radio telescope) will not radically limit the estimation of the effective generation parameter region.

In the considered region of stellar wind parameters, the plasma wave energy density W_2 , necessary for effective radio wave generation by Raman scattering, is much higher than by Rayleigh scattering. Therefore, the condition of effective radio wave generation $W \gg W_2$ is fulfilled only at extremely high velocity $v_{sw} \geq 1000$ km/s and concentration $n \geq 10^6 см^{-3}$ of the stellar wind (cf. Fig. 4 and Fig. 7).

When discussing the possibility of detecting radio emission on Earth, it is necessary to take into account that the Earth's ionosphere absorbs radio waves with frequencies below 10 MHz. Fig. 8 shows that radio emission at the basic plasma frequency passes through the ionosphere only at stellar wind concentrations above $n \geq 10^6 см^{-3}$, and at the doubled frequency - at concentrations above $2.5 \cdot 10^5 см^{-3}$.

Thus, due to frequency and energy limitations, registration of radio emission from the head shock wave of exoplanet HD 189733b on the Earth's surface is possible at stellar wind concentrations exceeding $n \geq 10^6 см^{-3}$. The frequency of radio emission is approximately equal to

the main plasma frequency, which is determined predominantly by the concentration and varies from 10 to 20 MHz at characteristic stellar wind parameters. For an extremely fast stellar wind, which has a velocity of $v_{sw} \gtrsim 1000$ km/s, radio wave generation at twice the plasma frequency is also possible and sufficiently efficient for registration by ground-based instruments.

6. CONCLUSION

In this work, we have studied the possibilities of the drift mechanism of electron acceleration as applied to the quasi-transverse head shock of exoplanet HD 189733b. In particular, we present estimates of the concentration, velocity, and energy density of the accelerated electron beam, which, given the characteristic parameters of the stellar wind in this system, turned out to be sufficiently high-energy to excite plasma waves.

On the other hand, the paper discusses the efficiency of the plasma mechanism of radio emission generation in the stellar wind near the head shock of exoplanet HD 189733b. The initial energy source in this mechanism is energetic electrons that excite plasma waves, which in turn, due to scattering, are converted into radio waves at the basic (Rayleigh scattering) or doubled (Raman scattering) plasma frequency. Therefore, a comparison of the energy of accelerated electrons with the minimum energy of plasma waves necessary for detection by modern radio telescopes on Earth of electromagnetic radiation allowed us to estimate the region of stellar wind parameters in which the registration of radio waves from an exoplanet head shock is energetically possible.

The efficiency of radio wave generation increases with increasing concentration and velocity and decreasing stellar wind magnetic field. It is also shown in this paper that at typical values of magnetic field, temperature, and stellar wind velocity in the HD 189733 system, the stellar wind concentration at the exoplanet head shock must exceed $n \gtrsim 10^6 \text{см}^{-3}$. to register radio waves at the main plasma frequency. If, in addition, the stellar wind velocity exceeds $v_{sw} \gtrsim 1000$ km/s, it is energetically possible to register radio waves at twice the plasma frequency. The most promising frequency range for radio wave detection lies near the ionospheric cutoff.

The work does not take into account the numerous factors that can enhance or weaken the radio emission from an exoplanet shock wave. Such factors include the specified size, location, shape, and type of the head exoplanet shock; possible refraction of radio waves in the HD 189733 system; **gyroabsorption (Stepanov et al., 1999)** and collisional absorption of radio waves during their propagation from source to receiver; different temperature of stellar wind electrons in the region of the shock wave from ions, etc. The study also considers the temperature of the stellar wind electrons in the region of the shock wave. The full electron velocity distribution function (15) obtained in this work is unstable not only with respect to Langmuir but also with respect to Weibel-type filamentation perturbations (Weibel, 1959; Bret et al., 2004; Kuznetsov et al., 2023). Their development can also significantly affect the generation of plasma waves and, consequently, radio

emission. The above-mentioned effects can significantly and to varying degrees affect the intensity of radio waves at both the main and doubled plasma frequencies, so both Rayleigh and Raman mechanisms may turn out to be capable of generating detectable radio emission, and the above effects require a detailed study in the future.

Of separate research interest is the application of other known accelerating mechanisms, such as the surfotron mechanism (Kichigin, 1995), to the plasma in the region of an exoplanet head shock.

The possible detection of radio emission could bring direct information on the properties of the exoplanet head shock and the stellar wind parameters in its vicinity. This could significantly refine existing gas-dynamic and magnetohydrodynamic models of the HD 189733 system and clarify the interaction of hot Jupiters with their parent stars.

FUNDING

This work was supported by grant No. 24-1-5-94-1 and grant No. 24-1-1-97-1 of the BASIS Foundation for the Development of Theoretical Physics and Mathematics.

CONFLICT OF INTERESTS

The authors declare that they have no conflict of interest.

REFERENCES

1. *Mikhailovsky A.B.* Theory of plasma instabilities. Moscow: Atomizdat, 1971. 276 p.
2. *Ball L., Melrose D.B.* Shock Drift Acceleration of Electrons // Publications of the Astronomical Society of Australia. 2001, vol. 18, pp. 361–373. DOI: 10.1071/as01047.
3. *Bourrier V., Lecavelier des Etangs A.* 3D model of hydrogen atmospheric escape from HD209458b and HD189733b: radiative blow-out and stellar wind interactions // Astronomy & Astrophysics. 2013, vol. 557, pp. A124. DOI: 10.1051/0004-6361/201321551.
4. *Bret A., Firpo M.-C., Deutsch C.* Collective electromagnetic modes for beam-plasma interaction in the whole//Physical Review E. 2004, vol. 70, pp. 046401. DOI: 10.1103/physreve.70.046401.
5. *De Hoffmann F., Teller E.* Magneto-Hydrodynamic Shocks // Physical Review. 1950, vol. 80, pp. 692–703. DOI: 10.1103/physrev.80.692.
6. *Dudík J. et al.* Nonequilibrium Processes in the Solar Corona, Transition Region, Flares, and Solar Wind (Invited Review) // Solar Physics. 2017, vol. 292, pp. 100. DOI: 10.1007/s11207-017-1125-0.
7. *Echim M.M., Lemaire J., Lie-Svendsen Ø.* A Review on Solar Wind Modeling: Kinetic and Fluid Aspects // Surveys in Geophysics. 2010, vol. 32, pp. 1–70. DOI: 10.1007/s10712-010-9106-y.

8. *Fares R. et al.* MOVES – I. The evolving magnetic field of the planet-hosting star HD189733 // Monthly Notices of the Royal Astronomical Society. 2017, vol. 471, pp. 1246–1257. DOI: 10.1093/mnras/stx1581.
9. *Ginzburg V.L.* The propagation of electromagnetic waves in plasmas. 1970.
10. *Goodrich C.C., Scudder J.D.* The adiabatic energy change of plasma electrons and the frame dependence of the cross-shock potential at collisionless magnetosonic shock waves // Journal of Geophysical Research: Space Physics. 1984, vol. 89, pp. 6654–6662. DOI: 10.1029/ja089ia08p06654.
11. *Grießmeier J., Zarka P., Girard J.N.* Observation of planetary radio emissions using large arrays // Radio Science. 2011, vol. 46, pp. RS0F09. DOI: 10.1029/2011RS004752.
12. *Holman G.D., Pesses M.E.* Solar type II radio emission and the shock drift acceleration of electrons // The Astrophysical Journal. 1983, vol. 267, pp. 837. DOI: 10.1086/160918.
13. *Kavanagh R.D. et al.* MOVES – II. Tuning in to the radio environment of HD189733b // Monthly Notices of the Royal Astronomical Society. 2019, vol. 485, pp. 4529–4538. DOI: 10.1093/mnras/stz655.
14. *Kichigin G.N.* Properties of surfatron acceleration of electrons // JETP. 1995, vol. 81, no. 4, pp. 736–744.
15. *Kuznetsov A.A. et al.* Saturating Magnetic Field of Weibel Instability in Plasmas with Bi-Maxwellian and Bikappa Particle Distributions // Plasma Phys. Rep. 2022, vol. 48, pp. 973–982. DOI: 10.1134/s1063780x22600700.
16. *Kuznetsov A.A. et al.* Quasilinear Simulation of the Development of Weibel Turbulence in Anisotropic Collisionless Plasma // Journal of Experimental and Theoretical Physics. 2023, vol. 137, pp. 966–985. DOI: 10.1134/s1063776123120099.
17. *Liu Z., Wang L., Guo X.* Acceleration of Solar Wind Suprathermal Electrons at the Earth's Bow Shock // The Astrophysical Journal. 2022, vol. 935, pp. 39. DOI: 10.3847/1538-4357/ac8157.
18. *Llama J. et al.* The Shocking Variability of Exoplanet Transits // Proceedings of the International Astronomical Union. 2013, vol. 8, pp. 262–265. DOI: 10.1017/s1743921313008521.
19. *Louis C.K. et al.* ExPRES: an Exoplanetary and Planetary Radio Emissions Simulator // Astronomy & Astrophysics. 2019, vol. 627, pp. A30. DOI: 10.1051/0004-6361/201935161.
20. *Mann G., Klassen A.* Electron beams generated by shock waves in the solar corona // Astronomy & Astrophysics. 2005, vol. 441, pp. 319–326. DOI: 10.1051/0004-6361:20034396.
21. *Mann G. et al.* Radio signatures of shock-accelerated electron beams in the solar corona //

Astronomy & Astrophysics. 2018, vol. 609, pp. A41. DOI: 10.1051/0004-6361/201730546.

22. *Melrose D.B., Hewitt R.G., Dulk G.A.* Electron-cyclotron maser emission: Relative growth and damping rates for different modes and harmonics // Journal of Geophysical Research: Space Physics. 1984, vol. 89, pp. 897–904. DOI: 10.1029/ja089ia02p00897.
23. *Odert P. et al.* Modeling the Ly transit absorption of the hot Jupiter HD 189733b // Astronomy & Astrophysics. 2020, vol. 638, pp. A49. DOI: 10.1051/0004-6361/201834814.
24. *Priest E.R.* Solar Magnetohydrodynamics. Springer Netherlands, 1982. ISBN 9789400979581. DOI: 10.1007/978-94-009-7958-1.
25. *Rumenskikh M.S. et al.* Global 3D Simulation of the Upper Atmosphere of HD189733b and Absorption in Metastable He i and Ly Lines // The Astrophysical Journal. 2022, vol. 927, pp. 238. DOI: 10.3847/1538-4357/ac441d.
26. *Shi C. et al.* Proton and Electron Temperatures in the Solar Wind and Their Correlations with the Solar Wind Speed // The Astrophysical Journal. 2023, vol. 944, pp. 82. DOI: 10.3847/1538-4357/acb341.
27. *Stepanov A.V. et al.* Second-Harmonic Plasma Radiation of Magnetically Trapped Electrons in Stellar Coronae //The Astrophysical Journal. 1999. vol. 524, № 2. pp. 961–973. DOI: 10.1086/307835
28. *Strugarek A. et al.* MOVES – V. Modelling star–planet magnetic interactions of HD 189733 // Monthly Notices of the Royal Astronomical Society. 2022, vol. 512, pp. 4556–4572. DOI: 10.1093/mnras/stac778.
29. *Treumann R.A., Baumjohann W.* Advanced Space Plasma Physics. Published by imperial college press, distributed by world scientific publishing co., 1997. ISBN 9781860943072. DOI: 10.1142/p020.
30. *Tsytovich V.N.* Theory of turbulent plasma. 1977.
31. *Vidotto A.A., Jardine M., Helling C.* Early uv ingress in wasp-12b: measuring planetary magnetic fieldS // The Astrophysical Journal. 2010, vol. 722, pp. L168–L172. DOI: 10.1088/2041-8205/722/2/L168.
32. *Weibel E.S.* Spontaneously Growing Transverse Waves in a Plasma Due to an Anisotropic Velocity Distribution // Phys. Rev. Lett. 1959, vol. 2, pp. 83–84. DOI: 10.1103/physrevlett.2.83.
33. *Wu C.S.* A fast Fermi process: Energetic electrons accelerated by a nearly perpendicular bow shock // Journal of Geophysical Research: Space Physics. 1984, vol. 89, pp. 8857–8862. DOI: 10.1029/ja089ia10p08857.
34. *Wu C.S., Lee L.C.* A theory of the terrestrial kilometric radiation // The Astrophysical Journal. 1979, vol. 230, pp. 621. DOI: 10.1086/157120.

35. *Yang L. et al.* Dynamic acceleration of energetic protons by an interplanetary collisionless shock // Astronomy & Astrophysics. 2024, vol. 686, pp. A132. DOI: 10.1051/0004-6361/202348723.
36. *Zaitsev V.V. et al.* Fast electrons in the plasmosphere of the exoplanet HD189733b // Geomagnetism and Aeronomy. 2024, vol. 64, (in press).
37. *Zaitsev V.V. et al.* On the Efficiency of Radio Emissions at the Double Plasma Frequency in the Magnetosphere of Exoplanet HD189733b // Geomagnetism and Aeronomy. 2023, vol. 63, pp. 892–898. DOI: 10.1134/s0016793223070307.
38. *Zaitsev V.V., Shaposhnikov V.E.* Plasma maser in the plasmasphere of HD189733b // Monthly Notices of the Royal Astronomical Society. 2022, vol. 513, pp. 4082–4089. DOI: 10.1093/mnras/stac1140.
39. *Zaitsev V., Stepanov A.* The plasma radiation of flare kernels // Solar Physics. 1983, vol. 88, pp. 1–2. DOI: 10.1007/bf00196194.
40. *Zheleznyakov V.V.* Radiation in Astrophysical Plasmas. Springer Netherlands, 1996. ISBN 9789400902015. DOI: 10.1007/978-94-009-0201-5.
41. *Zhilkin A.G., Bisikalo D.V.* On Possible Types of Magnetospheres of Hot Jupiters // Astronomy Reports. 2019, vol. 63, pp. 550–564. DOI: 10.1134/s1063772919070096.

Table 1. Stellar wind parameter sets used in the estimates.

Name of the set	N1	N2	N3	N4
v_{sw} km/s	240	235	480	1000
$n, см^{-3}$	10^5		$4.8 \cdot 10^5$	$4.4 \cdot 10^6$
T, K	10^6	10^6	$2.2 \cdot 10^6$	
B Gs	0.01	0.062	0.022	0.1
L , R_p			4.5	

Table 2. Results of electron acceleration efficiency estimates on the shock wave of exoplanet HD 189733b

Set name	N1	N2	N3	N4
α_{lc},°	42	43	37	32
$\frac{v_s}{v_{ms}}$	1.95	1.92	2.6	5.1
$n_{acc}(\theta_{max}), см^{-3}$		$1.7 \cdot 10^5$		$5.7 \cdot 10^5$
$v_{b,\parallel}(\theta_{max})$ km/s	$1.5 \cdot 10^4$	10^4	$2.06 \cdot 10^4$	$2.4 \cdot 10^4$
$v_b(\theta_{max})$, km/s	$1.8 \cdot 10^4$	$1.34 \cdot 10^4$	$2.35 \cdot 10^4$	$2.6 \cdot 10^4$
$W(\theta_{max})$	0.26	0.26	0.68	1.43

Table 3. Characteristics of radio emission generated by accelerated electron flows at different sets of parameters.

Name of the set	N1	N2	N3	N4
f_p MHz	3.2	21	6.9	20
W_1	0.16	0.03	0.06	0.01
W_2	28	0.14	1.26	0.16

FIGURE CAPTIONS

Fig. 1. Relation between the reference frame associated with the stellar wind and the de Hoffmann-Teller reference frame. The shaded area corresponds to reflected and accelerated electrons.

Fig. 2. Typical dependence of the dimensionless energy density of accelerated electrons $W(\theta)$ on the angle θ between the normal to the shock and the direction of the magnetic field.

Fig. 3. Dependence of the dimensionless maximum energy density of accelerated electrons $W(\theta_{max})$ on the pitch angle α_{lc}

Fig. 4. Dependence of the energy density of accelerated electrons $W(\theta_{max})$ on the concentration n at temperature $T = 1.5 \cdot 10^6$ K, magnetic field $B = 0.01$ Gs (black), $B = 0.04$ Gs (red), $B = 0.1$ Gs (blue), and stellar wind velocity $v = 250$ km/s (solid), $v = 500$ km/s (dashed), $v = 1000$ km/s (dotted).

Fig. 5. Approximate sensitivity of the ground-based radio telescopes LOFAR (solid), UTR-2 (dashed), and NDA (dotted).

Fig. 6. Dependence of the plasma wave energy density required to generate the $F = 0.01$ Yang radio wave flux on Earth by Rayleigh scattering W_1 on the concentration n at temperature $T = 1.5 \cdot 10^6$ K, magnetic field $B = 0.01$ Gs (black), $B = 0.04$ Gs (red), $B = 0.1$ Gs (blue), and stellar wind speed $v = 250$ km/s (solid), $v = 500$ km/s (dashed), $v = 1000$ km/s (dotted).

Fig. 7. Dependence of the plasma wave energy density required to generate the radio wave flux $F = 0.01$ Yang on Earth by Rayleigh scattering W_2 on the concentration n at temperature $T = 1.5 \cdot 10^6$ K, magnetic field $B = 0.01$ Gs (black), $B = 0.04$ Gs (red), $B = 0.1$ Gs (blue), and stellar wind speed $v = 250$ km/s (solid), $v = 500$ km/s (dashed), $v = 1000$ km/s (dotted).

Fig. 8. Dependence of the approximate frequency of radio emission generated via Rayleigh (solid) and Raman (dashed) plasma wave scattering on the stellar wind concentration at its temperature $T = 1.5 \cdot 10^6$ K. The dotted line shows the ionospheric cutoff frequency

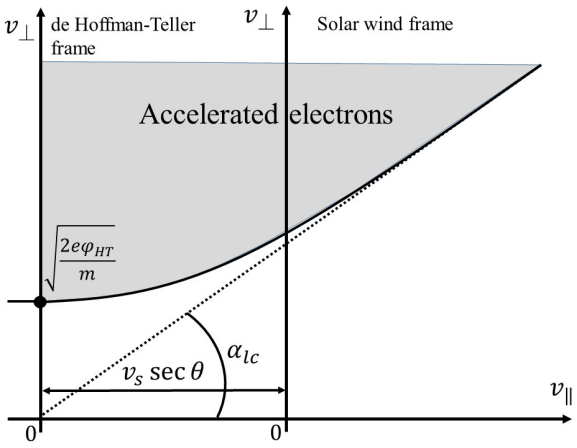
$v_\perp$
de Hoffman-Teller frame
$v_\perp$
Solar wind frame
Accelerated electrons
$\sqrt{\frac{2e\varphi_{HT}}{m}}$
α_{lc}
$v_s \sec\theta$
$v_\parallel$
0
0

Fig. 1.

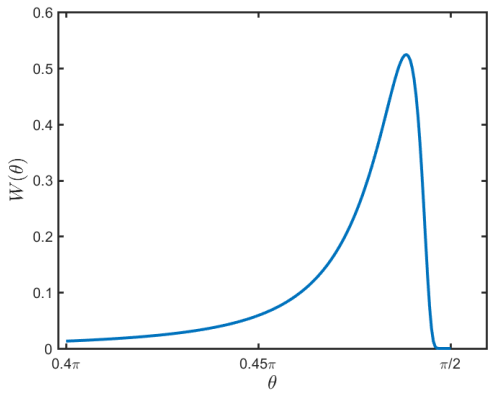
0.6
0.5
0.4
0.3
0.2
0.1
0
$W(\theta)$
0.4π
0.45π
π/2
θ

Fig. 2.

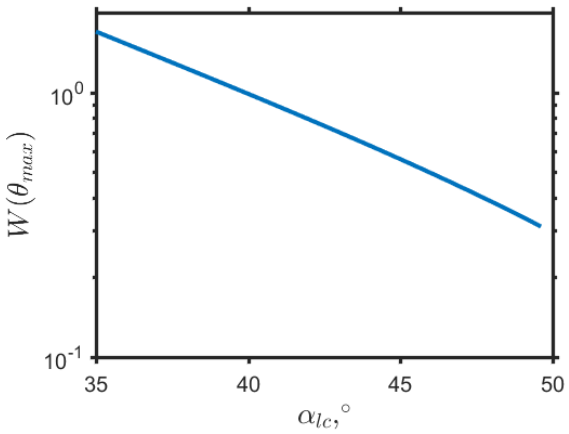
10^0
10^{-1}
$W(\theta_{max})$
35
40
45
50
$\alpha_{lc},^\circ$

Fig. 3.

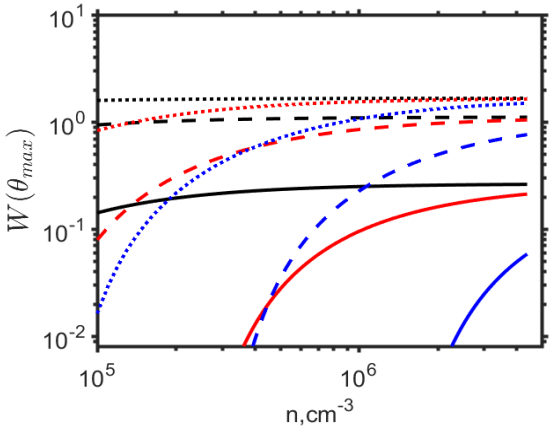
10^1
10^0
10^{-1}
10^{-2}
$W(\theta_{max})$
10^5
10^6
n,cm^{-3}

Fig. 4.

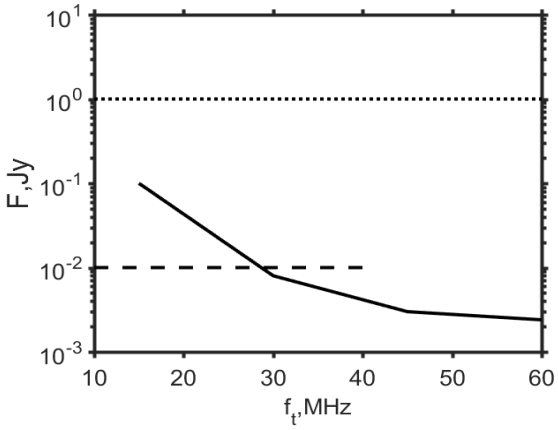
10^1
10^0
10^{-1}
10^{-2}
10^{-3}
F,Jy
10
20
30
40
50
60
f_t,MHz

Fig. 5.

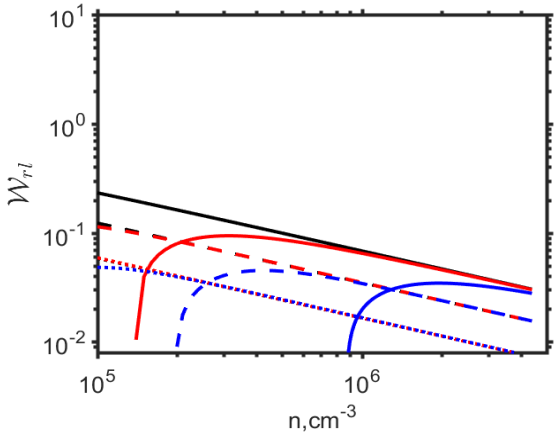
10^1
10^0
10^{-1}
10^{-2}
$\mathcal{W}_{rl}$
10^5
10^6
n,cm^{-3}

Fig. 6.

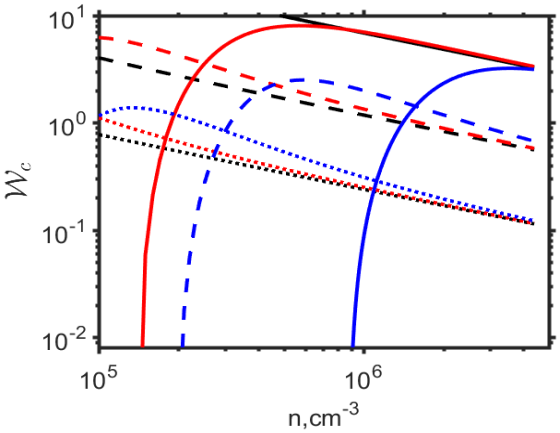

Fig. 7.

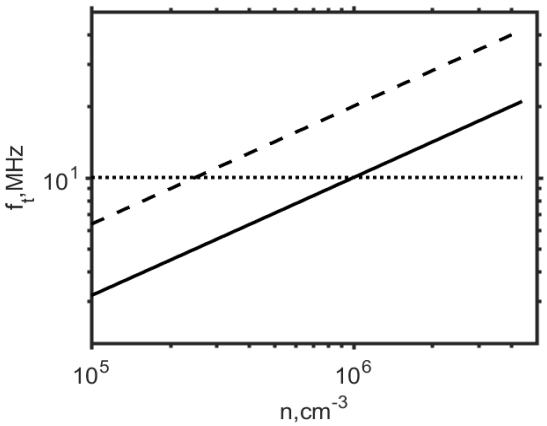

Fig. 8.